

Transport properties of a Wigner crystal in one- and two-dimensional asymmetric periodic potentials: Wigner crystal diode

Mikhail Y. Zakharov,¹ Denis Demidov,² and Dima L. Shepelyansky³

¹*Institute of Physics, Department of General Physics, Kazan Federal University, 42011 Kazan, Russia*

²*Kazan Branch of Joint Supercomputer Center, Scientific Research Institute of System Analysis, Russian Academy of Sciences, 42011 Kazan, Russia*

³*Laboratoire de Physique Théorique, IRSAMC, Université de Toulouse, CNRS, UPS, 31062 Toulouse, France*



(Received 15 January 2019; revised manuscript received 21 March 2019; published 18 April 2019)

We study the transport properties of a Wigner crystal in one- and two-dimensional asymmetric periodic potentials. We show that the Aubry transition takes place above a certain critical amplitude of potential with the sliding and pinned phase below and above the transition. Due to the asymmetry the Aubry pinned phase is characterized by the diode charge transport of the Wigner crystal. We argue that the recent experimental observations of Aubry transition with cold ions and colloidal monolayers can be extended to asymmetric potentials making it possible to observe a Wigner crystal diode with these physical systems and electrons on liquid helium.

DOI: [10.1103/PhysRevB.99.155416](https://doi.org/10.1103/PhysRevB.99.155416)

I. INTRODUCTION

The Wigner crystal of charged particles [1] occurs when the energy of their Coulomb repulsion exceeds the kinetic energy of their motion. The Wigner crystal appears in a variety of physical systems including electrons on a surface of liquid helium [2], electrons in two-dimensional (2D) semiconductor samples and one-dimensional (1D) nanowires (see, e.g., [3] and references therein), cold ions in radio-frequency traps [4,5], and dusty plasma in a laboratory or in space [6]. The Wigner crystal in a quasi-1D channel on liquid helium is also studied in experiments [7].

It is important to understand how the Wigner crystal is moving in a periodic potential in low-dimensional systems. The periodic potential can be viewed as a simplified description of a crystal potential created by atoms in a solid-state system. It also effectively appears in the frame of Little's suggestion [8,9] on electron conduction in long spine conjugated polymers with insights for possible synthesized organic superconductors. The properties of electron conduction in the regime of charge-density wave (CDW) are also related to the interacting charge propagation in a periodic potential which displays a host of unusual properties [10], including organic superconductivity [11,12].

The numerical and analytical analysis of properties of a 1D Wigner crystal in a periodic potential had been started in [13] with a proposal of experimental realization of this system with cold ions in optical lattices. It was shown that this system can be locally described by the Frenkel-Kontorova model [14] where the static positions of interacting particles are described by the Chirikov standard map [15]. This symplectic map captures many universal features of dynamical systems with a transition from the invariant Kolmogorov-Arnold-Moser (KAM) curves to a global chaotic diffusion when the last KAM curve is destroyed above the critical value of dimensional chaos parameter K [15–17]. As a result this

map describes the behavior of a variety of physical systems as depicted in [18]. In this frame of dynamical systems the irrational rotation number of the KAM curve corresponds to the fixed incommensurate density of particles in a periodic potential corresponding to incommensurate crystals [19].

The important step in the understanding of such incommensurate crystals was done by Aubry [20] showing that above the critical value of chaos parameter $K > K_c$ the KAM curve with an incommensurate rotation number is replaced by an invariant Cantor set, cantori, which has the minimal ground state energy configuration of interacting particles in the periodic potential. For $K < K_c$ the chain of particles has an acoustic spectrum of low energy phonon excitations corresponding to a sliding phase. In contrast, for $K > K_c$ the spectrum of excitations has an optical gap and the chain is pinned by the potential. The properties of low energy excitations for classical and quantum Wigner crystal are analyzed in [13,21,22] showing the existence of exponentially many low energy configurations in the proximity of the Aubry ground state. In a certain sense for $K > K_c$ the Aubry cantori ground state, which is mathematically exact, is hidden inside an exponentially large number of spin-glass-like configurations which are all populated in a physical system realization at finite temperature. For the Wigner crystal the pinned Aubry phase appears when the amplitude of the periodic potential exceeds a certain critical value measured in units of Coulomb interaction, while at small potential amplitudes, corresponding to the KAM curve, the crystal can easily slide in the potential.

In addition to the very interesting fundamental properties of the Aubry transition from sliding to pinning, it was established [23] that the pinned phase is characterized by the exceptional thermodynamic characteristics with a very large Seebeck coefficient and figure of merit $ZT > 3$ that exceeds the largest $ZT = 2.6$ value reached in material science experiments (see, e.g., review [24]).

After the proposal [13], the realizations of Wigner crystal of ions in optical lattices attracted the interest of experimental groups [25,26]. The signatures of the Aubry-like transition has been experimentally detected with a small number of cold ions by the group of Vuletic with about five ions [27]. The chains with a larger number of cold ions are experimentally studied in [28]. Two ion chains are used in [28] to create an effective periodic potential for ions in another chain (zigzag transition for ions is analyzed in [29]). Such a type of cold ion experiments can be considered as microscopic emulators of mechanisms of nanofriction in real materials as it is argued in [30–32].

Till now the cold ion traps are used to investigate mainly 1D or quasi-1D ionic Wigner crystal properties in periodic lattices. Recently a new step to the investigation of a 2D Wigner crystal in a periodic potential has been done with experimental observation of signatures of the Aubry transition using a colloidal monolayer on an optical lattice [33].

All previous studies considered the case of the periodic potential being symmetric in space with a sine shape. In this work we consider the case of an asymmetric potential with two harmonics which is relatively easy to realize with optical lattices (see, e.g., [34,35]). We also note that any crystal with three or more atoms in a periodic cell in general will generate an asymmetric potential. We show that in such a case a moderate static dc-field E_{dc} generates an asymmetric current corresponding to the Wigner crystal diode with a current flowing only in one direction. We study this diode current for the 1D case and 2D stripes of finite width. Due to the importance of diodes for electronic circuits (see [36] and overview in [37]) we assume that the obtained results will clarify the mechanisms of friction and transport on nanoscale.

II. MODEL DESCRIPTION

For the 1D case the Hamiltonian of the system of N interacting particles with equal charges in a periodic potential is given by

$$H = \sum_{i=1}^N \left(\frac{P_i^2}{2} + V(x_i) \right) + U_C, \quad (1)$$

$$U_C = \sum_{i>j} \frac{1}{\sqrt{(x_i - x_j)^2 + a^2}},$$

$$V(x_i) = K(\sin x_i + 0.4 \sin 2x_i).$$

Here x_i , P_i are a conjugated coordinate and momentum of particle i , and $V(x_i)$ is an external asymmetric periodic potential of amplitude K . We use the screened Coulomb interaction U_C between particles with the screening length a . Here we write the Hamiltonian in dimensionless units where the lattice period $\ell = 2\pi$ and the particle mass and charge are $m = e = 1$. In these atomiclike units the physical system parameters are measured in units: $r_a = \ell/2\pi$ for length, $\epsilon_a = e^2/r_a = 2\pi e^2/\ell$ for energy, $E_{adc} = \epsilon_a/er_a$ for the applied static electric field, $v_a = \sqrt{\epsilon_a/m}$ for particle velocity v , and $t_a = er_a\sqrt{m}/\epsilon_a$ for time t .

For the 2D case the Hamiltonian has the same form with

$$H = \sum_{i=1}^N \left(\frac{P_{ix}^2}{2} + \frac{P_{iy}^2}{2} + V(x_i, y_i) \right) + U_C,$$

$$U_C = \sum_{i>j} \frac{1}{\sqrt{(x_i - x_j)^2 + (y_i - y_j)^2 + a^2}}, \quad (2)$$

$$V(x_i, y_i) = K(\sin x_i + 0.4 \sin 2x_i - \cos y_i),$$

and 2D momentum P_{ix} , P_{iy} conjugated to x_i , y_i .

Similar to [23] the dynamics of interacting charges is modeled in the frame of the Langevin approach (see, e.g., [38]) with the equation of motion in 1D being

$$\dot{P}_i = \dot{v}_i = -\partial H/\partial x_i + E_{dc} - \eta P_i + g\xi_i(t), \quad \dot{x}_i = P_i = v_i. \quad (3)$$

The parameter η phenomenologically describes the dissipative relaxation processes, and the amplitude of Langevin force g is given by the fluctuation-dissipation theorem $g = \sqrt{2\eta T}$. Here we also use particle velocities $v_i = P_i$ (since mass is unity). As usual, the normally distributed random variables ξ_i are defined by correlators $\langle \xi_i(t) \rangle = 0$, $\langle \xi_i(t)\xi_j(t') \rangle = \delta_{ij}\delta(t - t')$. The amplitude of the static force is given by E_{dc} . For the 2D case the equations of motion have the same form with the force E_{dc} acting in x direction.

The length of the system in the 1D case is taken to be $2\pi L$ in x direction with L being the integer number of periods with periodic boundary conditions. In 2D we studied the case of stripes with the width of $2\pi N_s$ considering usually up to $N_s = 5$ period cells in y direction with periodic boundary conditions.

The numerical simulations are based on the combination of Boost.odeint [39] and VexCL [40,41] libraries and employed the approach described in [42] in order to accelerate the solution with NVIDIA CUDA technology. Problem (1) is solved using the fourth-order Runge-Kutta method and (2) by the Verlet method, where each particle is handled by a single GPU thread. Since Coulomb interactions in U_C are decreasing with distance between particles, the interactions for the 2D case were cut off at the radius $R_C = 6\ell = 12\pi$ that allowed us to reduce the computational complexity of the algorithm from $O(N^2)$ to $O(N \log N)$. In 1D in some cases we only considered interactions between immediate left and right neighbors, since, as shown in [13,23], the contribution of other particles does not play a significant role. In all simulations, in order to avoid close encounters between particles leading to numerical instability, the screening length $a = 0.7$ is used. At this value of a the interaction energy is still significantly larger than the typical kinetic energies of particles ($T \ll 1/a$) and the screening does not significantly affect the interactions of particles. We usually employed the relaxation rate $\eta = 0.1$ being relatively small compared to typical oscillation timescales in the system, but other values of η were also considered. The source code for the 1D and 2D experiments is available at <https://gitlab.com/ddemidov/thermoelectric1d> and <https://gitlab.com/ddemidov/thermoelectric2d> correspondingly. The numerical simulations were run at OLYMPE CALMIP cluster [43] using NVIDIA Tesla V100 GPUs and partially at Kazan Federal University using NVIDIA Tesla C2070 GPUs.

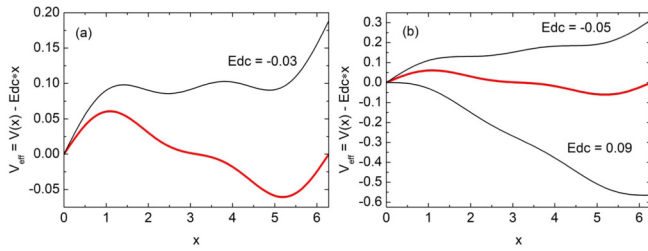


FIG. 1. The effective static potential $V_{\text{eff}}(x) = V(x) - E_{\text{dc}}x$ for one charge is shown by black and red/gray curves in the presence of a static force E_{dc} at $K = 0.05$, the red/gray curve corresponds to $E_{\text{dc}} = 0$; the black curves show nonzero values of E_{dc} in (a) and (b).

III. STATIC CONFIGURATIONS AND AUBRY TRANSITION

We start from the analysis of properties of static configurations of particles in the 1D case. The effective potential $V_{\text{eff}} = V(x) - E_{\text{dc}}x$, acting on a particle in presence of a static force E_{dc} , is shown in Fig. 1. At $E_{\text{dc}} = 0$ there is one potential minimum. In the presence of the static force E_{dc} there are no potential minima for the force $E_{\text{dc}} > -K$ pushing to the left and $E_{\text{dc}} < 1.8 K$ pushing to the right. Thus the asymmetry of the potential leads to different sliding borders for the left and right force acting on one particle. This asymmetry is at the origin of diode transport of the Wigner crystal.

At $E_{\text{dc}} = 0$ the static configurations of the Wigner crystal energy local minima are defined by the conditions $\partial H/\partial x_i = 0$ [13,14,20]. As discussed in [13], in the approximation of nearest neighbor interacting charges, these conditions lead to the dynamical symplectic Wigner map for equilibrium positions x_i of charges in the Wigner crystal (with $P_i = v_i = 0$):

$$p_{i+1} = p_i + Kg(x_i), \quad x_{i+1} = x_i + 1/\sqrt{p_{i+1}}, \quad (4)$$

where the effective momentum conjugated to x_i is $p_i = 1/(x_i - x_{i-1})^2$ and the kick function $Kg(x) = -dV(x)/dx = -K(\cos x + 0.8 \cos 2x)$.

To check the validity of the map description we find the ground state configuration using numerical methods of energy minimization described in [13,20]. Here the Coulomb interaction between all electrons is used in the numerical simulations. We use the hard wall boundary conditions at the ends of the chain (for ions they can be created by specific laser frequency detuning from resonant transition between ion energy levels). This leads to the density ν of charges along the chain being inhomogeneous since a charge in a boundary vicinity has more pressure from other charges in the chain (a similar inhomogeneous local density $\nu(x_i) = 2\pi/|x_{i+1} - x_i|$ appears for ions inside a global oscillator potential of a trap as discussed in [13]). Thus, as in [13], we select the central part of the chain with approximately 1/3 of all charges where the density is approximately constant being close to the golden mean value $\nu = \nu_g - 1 = (\sqrt{5} - 1)/2 \approx 0.618$ [or $\nu = \nu_g = (\sqrt{5} + 1)/2 \approx 1.618$] which is assumed

to be a most robust KAM curve for the Chirikov standard map [16,17,20]. This choice corresponds to an incommensurate phase with the golden KAM curve usually studied for the Aubry transition [16,17,20].

The numerically obtained charge positions and momentum x_i, p_i are shown in Fig. 2 for $\nu \approx 0.618$ (see Fig. 13 in the Appendix for $\nu \approx 1.618$). From the numerical values x_i we determine the kick function $g(x)$ which is close to the theoretically expected relation $Kg(x) = -dV/dx$ shown by the dashed curve. For small potential amplitudes $K < 0.0015$ the chain is in the sliding phase with a continuous KAM curve in the Poincaré section plane (x, p) . For $K > 0.0015$ the points (x_i, p_i) start to be embedded inside the chaotic component of the phase plane corresponding to the Aubry pinned phase. In this phase the points (x_i, p_i) form a fractal Cantor set in the phase plane and the chain is pinned by the potential. According to the data of Fig. 1 the Aubry transition from sliding to pinned phase takes place at the critical value $K_c \approx 0.0015$. The qualitative change of chain properties with the transition from sliding to pinned phase can be also seen with the help of the hull function $h(x)$ which gives the charge positions in a periodic potential vs unperturbed positions at $K = 0$ both taken as $\text{mod } 2\pi$. For $K < K_c$ we have a continuous function $h(x) \approx x$ while for $K > K_c$ the hull function has a form of devil's staircase with charge positions clustering near certain values. For $\nu \approx 1.618$ we find $K_c \approx 0.015$ (see Fig. 13 in the Appendix).

For the potential $V(x) = -K \cos x$ the Wigner map (4) can be locally described by the Chirikov standard map as it is explained in [13]. This gives the Aubry transition at the potential amplitude

$$K_{cv} \approx 0.034(\nu/\nu_g)^3, \quad \nu_g = 1.618 \dots \quad (5)$$

At $\nu = 1.618 \dots$ the numerical results obtained in [13,23] give $K_c \approx 0.0462$ that is slightly above the theoretic value. We attribute this modest difference to an inhomogeneous density of resonances in (4) (the Chirikov standard map approximation assumes it to be constant [15]) and to nearest neighbor interactions between charges present in the Wigner crystal. The recent results confirm the cubic decrease of K_{cv} with charge density ν [44].

In our case with two harmonics of potential the density of resonances is increased which, according to the Chirikov criterion of overlapped resonances, should decrease K_c value (see [15,16]). Indeed, for $\nu = 1.618$ we have $K_c \approx 0.015$ being approximately 3 times smaller compared to the case of one harmonic potential with $K_c \approx 0.0462$. For $\nu \approx 0.618$ we have $K_{cv} \approx 0.0015$ while the cubic extrapolation like in (5) gives $K_{cv} \approx 0.00084$ being by 40% lower than the numerical values from Fig. 2. We consider this as satisfactory taking into account the approximate K_c values extracted from Figs. 2 and 13. Thus for the potential (1) we have on average the density dependence of the critical potential amplitude of the Aubry transition: $K_{cv} \approx 0.01(\nu/\nu_g)^3$.

We note that the significant decrease of K_c for the two harmonic potential and especially with density ν can be rather important for experiments with optical lattices since a smaller potential amplitude is more accessible with low power lasers.

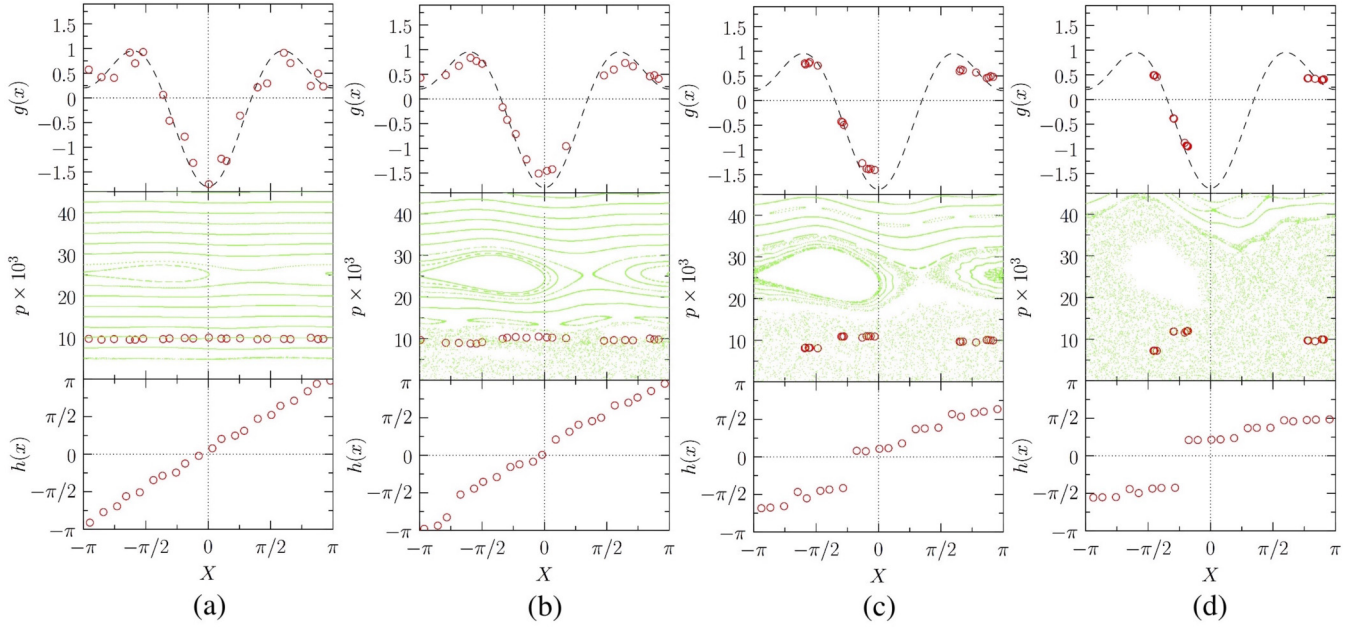


FIG. 2. Functions related to the dynamical map (4) obtained from the ground state equilibrium positions x_i of $N = 61$ charged particles for $L = 90$ potential periods (with hard wall boundary conditions) for density $\nu \approx 0.618$ in the central chain part at $K = 0.0002$ (a), $K = 0.001$ (b), $K = 0.002$ (c), and $K = 0.005$ (d) (charges are marked by open circles). In each panel the top subpanel shows the kick function $g(x)$ (dashed curve is the theoretical curve, circles are actual charge positions); the middle subpanel shows the Poincaré section of map (4) (green/gray points) and actual charge positions (x_i, p_i) (open circles); and the bottom subpanel shows the hull function $h(x)$ (see text). The charge positions are shown as $x = x_i \pmod{2\pi}$ for the central 1/3 part of the chain.

IV. DIODE TRANSPORT IN 1D

The charge transport is computed with N charges on L potential periods with periodic boundary conditions (here we consider Coulomb interactions only between nearest neighbor charges as discussed in Sec. II). We compute the velocity $v(t)$ of a chain at time t as an average velocity of all N charges at that time moment. A typical dependence of $v(t)$ on time is shown in Fig. 3. The system parameters correspond to the Aubry pinned phase. We see that approximately for $t > 100$ the motion of a chain is in a stationary regime with its steady-state propagation along the potential under the applied static force E_{dc} . The velocity of Wigner crystal propagation v_W to the left is close to the velocity of a free particle in the presence of force and dissipation $v_0 = E_{dc}/\eta = 0.47$ for the case of Fig. 3. The time averaged value $v_{left} = 0.439$ is a bit smaller than v_0 showing that the potential slightly decreases the propagation velocity. In contrast, the chain propagation to the right has a significantly smaller velocity $v_{right} = 0.089 \ll v_0$ for the same amplitude of static force. Also instantaneous values of velocity $v(t)$ have significant fluctuations with an even almost zero velocity at some moments of time. This data clearly demonstrate the emergence of diode transport in the asymmetric potential in the presence of interactions. From the physical viewpoint the velocity to the right is smaller than to the left since the potential has a steep slope in this direction while moving to the left a particle follows a gentle slope. Thus in winter it is easier to pull a sleigh along a gentle slope of a hill than along a steep slope even if the hill height is the same from both sides.

The dependence of Wigner crystal velocity v_W on E_{dc} is shown in Fig. 4 for the Aubry pinned phase at $K = 0.05$ and

$\nu = N/L \approx 0.618$ for different values of temperature T . At small $T = 0.1K_c = 0.00462 \ll K = 0.05$ we have a strongly asymmetric diode transport appearing at finite E_{dc} fields. With the increase of temperature the diode transport becomes less and less pronounced. Indeed, when the temperature is comparable with the potential height, e.g., $T = 0.8K_c \approx 0.037$

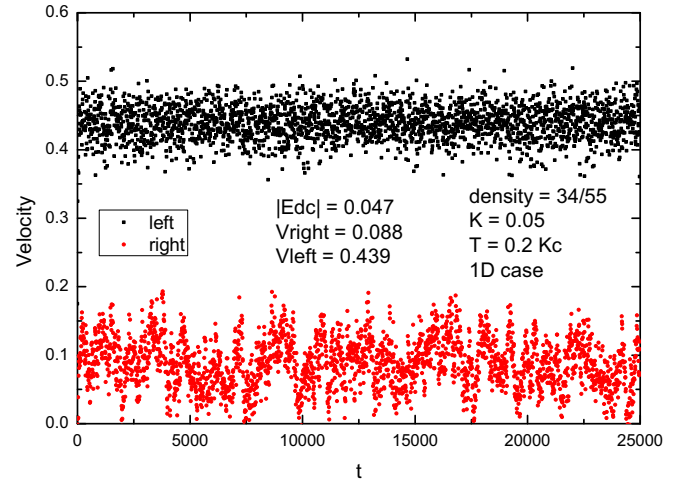


FIG. 3. Dependence of average chain velocity $v(t)$ at time t in 1D for $N = 34$ particles and $L = 55$ periods of potential (with periodic boundary conditions $\nu = 34/55$). Here $E_{dc} = -0.047$ (black points) with time average Wigner crystal velocity $v_W = v_{left} = -0.439$ and $E_{dc} = 0.047$ (red/gray points) with time average $v_W = v_{right} = 0.088$; the system parameters are $K = 0.05$, $T = 0.2K_c$, $K_c = 0.0462$, $\eta = 0.1$ (time averaging is done over times above 1/2 of the whole time interval).

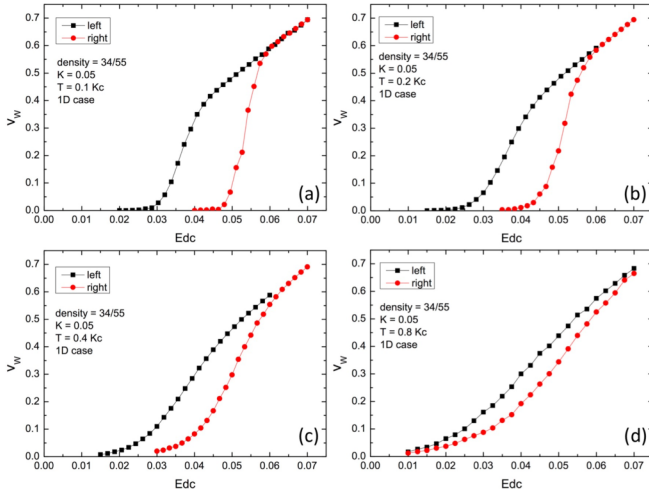


FIG. 4. Dependence of Wigner crystal velocity v_W , averaged over times $t \leq 10^4$, on static field amplitude E_{dc} for propagation to the left (black points) and to the right (red/gray points). Here $\nu = N/L = 34/55$, $K = 0.05$, $\eta = 0.1$ and temperature $T/K_c = 0.1, 0.2, 0.4$, and 0.8 for (a), (b), (c), and (d), respectively. Here $K_c = 0.0462$ is the critical amplitude of Aubry transition for $\nu = 1.618\dots$ in a potential with one harmonic [13,23].

$\sim K = 0.05$, the statistical Boltzmann fluctuations over a potential barrier smooth the asymmetry of transport. In this regime at small E_{dc} fields the velocities to the left and to the right directions become the same as it is shown in Fig. 5.

Indeed, in the linear regime limit at $E_{dc} \rightarrow 0$ the principle of the detailed balance (see, e.g., [45]) guarantees that the flow is the same in both directions. We note that this point had been discussed in detail by Feynman for a case of asymmetric potential [46] which became known as ratchet. Indeed, as we show below (see Sec. VII) at small temperatures the dependence $v_W(T)$ is well described by the Arrhenius thermal activation equation. At present, the term *ratchet*, discussed by Feynman, is used more for a description of directed transport appearing in an asymmetric periodic potential under a time-periodic force driving (see, e.g., [47–49]). Due to these reasons we use the term diode which is more adequate for

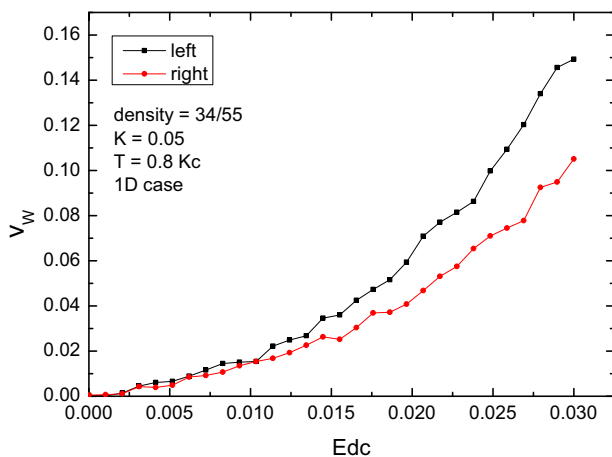


FIG. 5. Zoom of Fig. 4(d) at small E_{dc} .

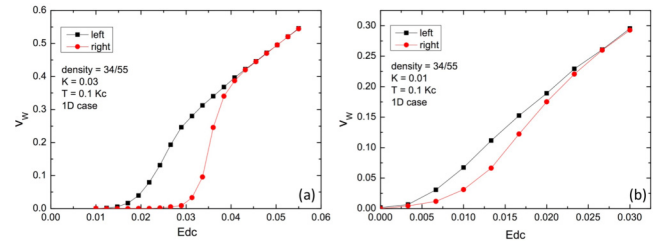


FIG. 6. Same as in Fig. 4(a) but at $K = 0.03$ (a) and $K = 0.01$ (b).

the case of static force without any time-periodic driving. It directly corresponds to the asymmetry of charge flow obtained in our model.

At fixed temperature [e.g., at $T = 0.1K_c$ as in Fig. 4(a)] the asymmetry of diode transport decreases with a decrease of the potential amplitude K as it is shown in Fig. 6. Indeed, with a decrease of K the potential height becomes comparable with temperature and, as above, the principle of detailed balance leads to the same flows in both directions.

The influence of Coulomb interactions of the diode transport is obtained from the comparison of Figs. 7(a), 4(a), and 7(b) where the electron density takes values $\nu = N/L = 21/55, 34/55$, and $34/21$, respectively, with all other parameters kept fixed. All these three cases are located in the pinned phase. We see that at $N/L = 21/55$ and $34/55$ the diode velocity dependence $v_W(E_{dc})$ on E_{dc} remains practically the same. We explain this by the fact that at small densities the interactions between charges become weak compared to the periodic potential and thus we approach the limit of transport of noninteracting particles which still demonstrates the diode flow due to potential asymmetry. The opposite tendency appears with the increase of density to $N/L = 34/21$. In this case the interactions are strong, even if we are still in the pinned phase, and the asymmetry of potential is less pronounced so that the transport flows are close to be symmetric even if one still needs to apply a finite force $E_{dc} \approx 0.02$ to obtain moderate velocities of Wigner crystal motion along the periodic potential. This force can be interpreted as the static friction force $F_s \approx E_{dc} \approx 0.02$. We note that with the increase of interactions (or density) we have a reduction of F_s values. Indeed, at lower density $N/L = 34/55$ we have larger values of static friction force $F_s \approx 0.03$ (for left direction) and $F_s \approx 0.05$ (for right direction). Indeed, with an increase of interactions we approach the sliding phase [the border of Aubry transition is growing this density (5) where $F_s = 0$].

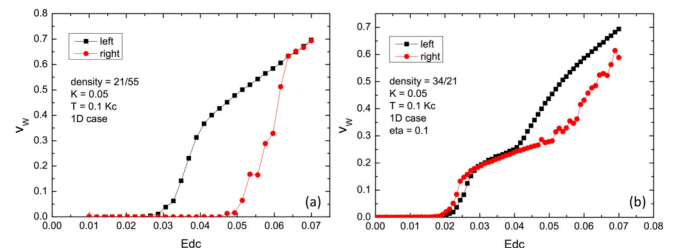


FIG. 7. Same as in Fig. 4(a) but for different electron densities $N/L = 21/55$ (a) and $N/L = 34/21$ (b).

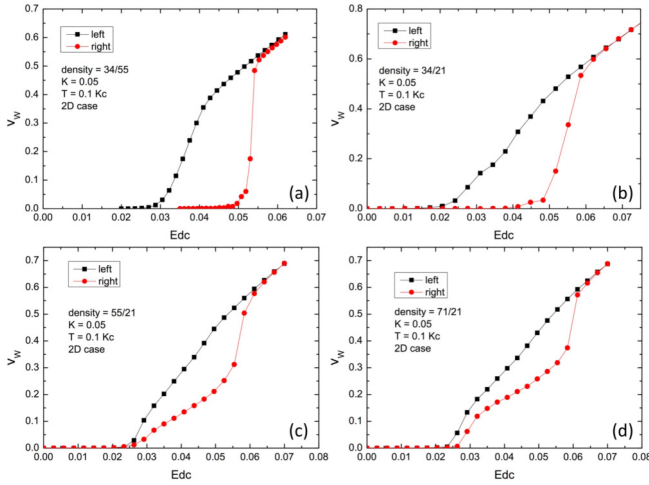


FIG. 8. Dependence of Wigner crystal velocity v_W on E_{dc} in the 2D case (five lines in the transverse y direction) at densities $\nu = N/L = 34/55$ (a), $34/21$ (b), $55/21$ (c), and $71/21$ (d). Other system parameters are as in Fig. 4(a).

We note that for $E_{dc} < F_s$ the Wigner crystal velocity v_W happens due to the Arrhenius thermal activation (see Sec. VII) so that it drops exponentially with a decrease of temperature. In contrast, for $E_{dc} > F_s$ we have a rather weak change of v_W with T (see, e.g., Fig. 4).

The above results are presented for the dissipation rate $\eta = 0.1$. We tested also smaller values of η for which we obtained qualitatively similar results. Thus for parameters of Fig. 7(b) we have an approximately similar shape of $v_W(E_{dc})$ dependence for $\eta = 0.1$ and $\eta = 0.02$ (see Fig. 14) with a more sharp shape in the latter case with a smaller value $F_s \approx 0.013$. We argue that at smaller dissipation statistical fluctuations at a given temperature have more possibilities to overcome potential barriers that leads to a moderate decrease of F_s .

V. DIODE TRANSPORT IN 2D

The diode properties of the Wigner crystal in 2D are studied with the Hamiltonian (2) and related Langevin equations (3). We use periodic boundary conditions in x and y directions with the static field E_{dc} always acting in x direction. The majority of the results were obtained with five cells in y giving us $N_s = 5$ stripes along x with one periodic cell in each stripe (we obtained very similar results with only $N_s = 1$ stripe in y). We keep the same density $\nu = N/L$ in each stripe as in the above 1D case. Thus the total number of charges is $N_{tot} = N_s N$ with L and N_s potential periods in x and y . Similar to the 1D case (see Fig. 2) we compute the local average charge velocity $v(t)$ in x direction at instant time moment t by averaging over all N_{tot} charges [an example of dependence $v(t)$ is shown in Fig. 15]. In 2D simulations we usually used timescales up to $t = 5 \times 10^4$ when the crystal propagation is well stabilized.

The dependence of Wigner crystal velocity v_W of E_{dc} in 2D is shown in Fig. 8 at different densities $\nu = N/L = 34/55$, $34/21$, $55/21$, and $71/21$ with all other parameters kept fixed being also the same as in the corresponding 1D cases. At low density $N/L = 34/55$ the dependence $v_W(E_{dc})$

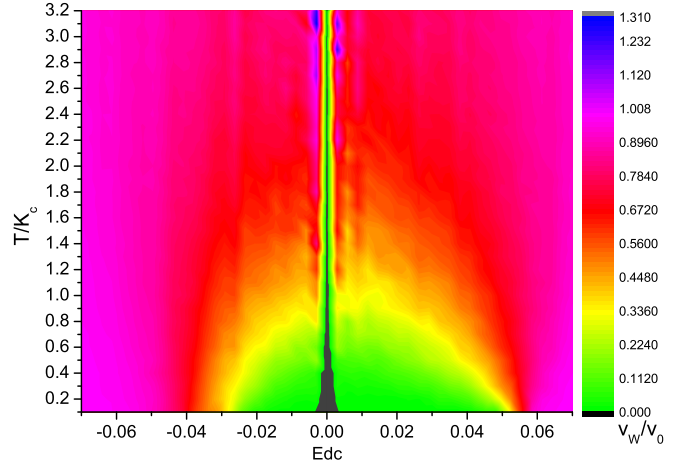


FIG. 9. Dependence of v_W/v_0 , shown by color, on T/K_c and E_{dc} for the 2D case with five stripes and $N/L = 34/21$, $K = 0.05$, $K_c = 0.0462$, $\eta = 0.1$, $v_0 = E_{dc}/\eta$.

remains practically the same in 1D and 2D. We attribute this to relatively weak interactions between charges so that the diode transport is rather close to the noninteracting case. The situation is drastically different for $N/L = 34/21$: in 1D the diode transport asymmetry is quite weak [Fig. 7(b)] while in 2D we have a strong asymmetry [Fig. 8(b)] with different values of static friction force $F_s \approx 0.025$ (left) and $F_s \approx 0.05$ (right). At larger densities $N/L = 55/21$ and $71/21$ the asymmetry is reduced due to an increase of interactions with $F_s \approx 0.025$ for both directions. Thus in the 2D case we have a tendency similar to the 1D case with a reduction of diode transport asymmetry with the density increase.

The global dependence of 2D Wigner crystal velocity $|v_W|$ on temperature T and E_{dc} is shown in Fig. 9 for density $\nu = N/L = 34/21$. We find that the diode transport is well visible for temperatures being smaller than the potential height $T/K_c \approx T/K < 1$ where v_W is significantly smaller than $v_0 = E_{dc}/\eta$. At large T/K_c values v_W becomes close to v_0 since in this regime the potential influence becomes small. Of course, at very small E_{dc} values the velocity v_W becomes very small and it becomes difficult to determine exactly very small v_W values in numerical simulations on a finite timescale (here v_W appears due to exponentially rare thermal fluctuations). This is at the origin of the peaklike structure near $E_{dc} \approx 0$ in Fig. 9.

Overall, the results for diode transport in 2D show that its properties are similar to those of the 1D case.

We note that using GPUs in the numerical experiments allows us to make simulations with a significantly larger number of particles going up to $N_{tot} \sim 10^4$ without a significant increase of computational times. However, this work was focused on analysis of specific physical effects related to diode transport for which it was sufficient to stay within a maximal $N_{tot} = 445$ (see below). Recently, the numerical simulations of the 2D Wigner crystal in a spatially modulated system with up to 1600 charges has been reported in [50]. However, the possible links with the Aubry transition have been not discussed in this work. We think that without such links it is rather difficult to understand the physics of various dislocation phases appearing in 2D.

Another thing worth mentioning is the possibility of realization of thermal diode discussed in [51]. On first glance it seems natural that in the presence of a charge diode transport one can expect the thermal diode flow to appear in our model. However, we were not able to find a thermal diode regime in our model. We explain this by the fact that the charge diode transport appears at finite E_{dc} field values. Such fields are rather moderate on a local scale but for a large system size they correspond to a significant voltage difference ΔV_{dc} applied to the sample. In contrast, the temperature difference applied to the sample is always smaller than the sample temperature and due to that to long sample the temperature gradient becomes very small so that, due to the detailed balance [45], the left and right heat flows remains equal in this linear limit of small temperature gradient.

In the next section we characterize the structure of the moving the Wigner crystal in 2D.

VI. FORM FACTOR OF MOVING A WIGNER CRYSTAL

To characterize the structure of a Wigner crystal in moving and static regimes we use the form factor defined as

$$F(k) = \langle |\text{Re} \sum_{i \neq j}^{N_{\text{tot}}} \exp\{ik[x_i(t) - x_j(t)]\}|^2 \rangle / N_{\text{tot}}, \quad (6)$$

where the average is done over all particles and ten different moments of time homogeneously spaced on the whole computational interval of time. A similar approach had been used in [13]. It showed that the form factor captures the Aubry transition from sliding phase with $F(k)$ peaks at incommensurate values $k \approx \nu j$ with integer j while in the pinned phase the peaks are more pronounced at $k \approx j$ corresponding to the lattice period (see Fig. 5 in Ref. [13]). Of course, in the pinned phase the density is still incommensurate (e.g., $\nu = 1.618 \dots$) but the charges are clustered in groups where their positions are more closely located to potential minima with some displacements (dislocations) between clusters due to the fractal devil's staircase structure of the whole chain in the pinned phase. These clusters give peaks of $F(k)$ at $k \approx j$.

For the static Wigner crystal at $E_{dc} = 0$ we also find a similar $F(k)$ structure shown in Figs. 10(a) and 10(b) for sliding and pinned phases, respectively. However, in the sliding phase at $K = 0.001 \ll K_c$ we have $F(k)$ peaks located at $k \approx \nu_{\text{eff}} j$ with $\nu_{\text{eff}} \approx \sqrt{\nu} \approx 1.272$. Indeed, in 2D the average distance between particles becomes $1/\sqrt{\nu}$ instead of $1/\nu$ as it was in the 1D case. Due to that we find peaks at $k \approx \sqrt{\nu} j$ in Fig. 10(a). In contrast, in the pinned phase the periodic potential imposes peaks at $k \approx j$ in Fig. 10(b).

The form factor of the moving Wigner crystal in the diode regime at $E_{dc} = -0.03$ and -0.045 is shown, respectively, in Figs. 10(c) and 10(d) for the pinned phase. The main peaks are still located at integer $k \approx j$ even though they are somewhat broadened due to fluctuations of changes during their propagation along the lattice. These fluctuations mainly affect large peaks at large $j = 3, 4, \dots$ but the peaks at $j = 1, 2$ remain. It is important to note that with the increase of the ring size going from $N/L = 34/21$ to $N/L = 89/55$ we recover the same form factor structure. This shows that the

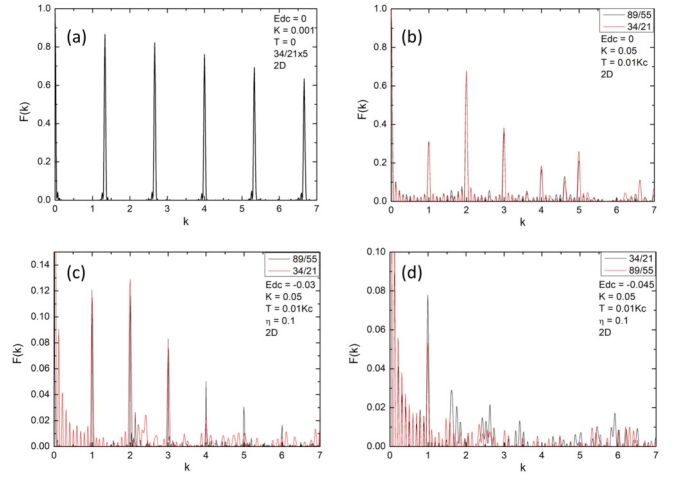


FIG. 10. Form factor $F(k)$ in the 2D case with five stripes for (a) $N/L = 34/21$, $K = 0.001$, $T = 0$ (η is not important since $E_{dc} = 0$); (b) $N/L = 34/21$, $89/55$, $K = 0.05$, $T = 0.01K_c$ (η is not important since $E_{dc} = 0$); (c) same as (b) but at $E_{dc} = -0.03$, $\eta = 0.1$; and (d) same as (b) but at $E_{dc} = -0.045$, $\eta = 0.1$.

chosen system size corresponds to the thermodynamic limit of the infinite system.

The dependence of $F(k)$ on temperature T for a moving crystal at $E_{dc} = -0.03$ is shown in Fig. 11. With the increase of T the fluctuations become stronger and the peaks are suppressed at large $T/K_c \approx T/K$ values. However, the peaks at $k \approx j = 1, 2$ remain rather robust even at large T/K .

The dependence of the form factor on E_{dc} at fixed temperature is shown in Fig. 12. At moderate $|E_{dc}| < 0.05$ values in the diode regime we have $F(k)$ peaks mainly at $k \approx j = 1, 2, 3, 4, 5, 6$ (they are more pronounced for large size with five stripes). But at a stronger field $|E_{dc}| > 0.05$ we see a transition to incommensurate structure with peaks located at $k \approx \tilde{\nu} j$ with $\tilde{\nu} \approx 1.5$ corresponding to an intermediate density between $\nu_{\text{eff}} \approx 1.272$ and $\nu = 1.618$. Thus a sufficiently strong dc field can change the structure of the moving pinned Wigner crystal to the sliding incommensurate crystal. Indeed,

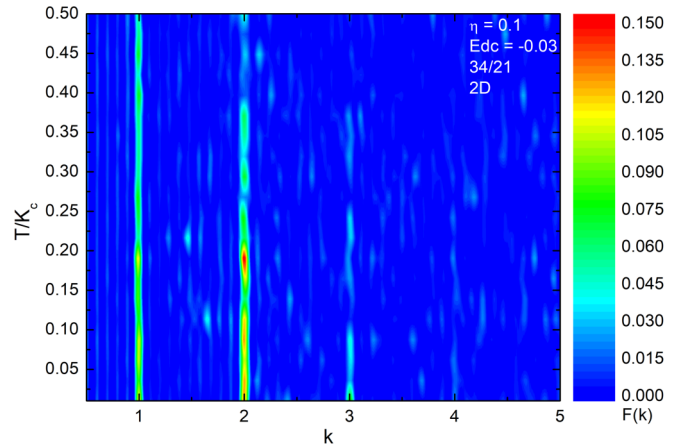


FIG. 11. Dependence of form factor $F(k)$, shown by color, on T/K_c and k ; $N/L = 34/21$, $\eta = 0.1$, $E_{dc} = -0.03$ in 2D with five stripes.

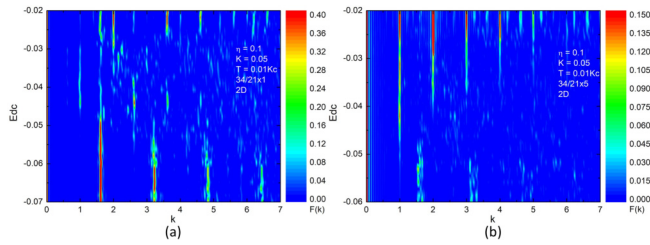


FIG. 12. Dependence of form factor $F(k)$ of a moving Wigner crystal on E_{dc} and k for $K = 0.05$, $T = 0.01K_c$, $K_c = 0.0462$, $\eta = 0.1$ in 2D at $N/L = 34/21$ with one stripe (a) and with five stripes (b) [color bar marks $F(k)$ values].

at strong E_{dc} the crystal velocity v_W becomes rather large and the periodic potential gives to this directed flow only relatively weak perturbation.

We present the video of Wigner crystal motion in the diode regime in the Supplemental Material [52].

VII. ANALYSIS OF APPROXIMATIONS

The performed numerical simulations use certain approximations like, e.g., the Langevin approach for the thermal bath, finite interaction range between charges. Here we briefly justify the validity of these approximations.

Thus, in Fig. 16 we show the velocity distributions in 1D and 2D cases. These results show that the numerical results well reproduce the theoretical thermal Maxwell distribution centered at the average particle velocity v_W . At significant values of E_{dc} and related v_W there is a noticeable deformation of the distribution which we attribute to a moderate heating of particles by the static force E_{dc} and effects of their interactions in the presence of a periodic potential. However, we note that even when there is a visible deformation of the distribution in x direction in the 2D case, the distribution in y direction is still very well described by the Maxwell one. We note that as it was described Sec. II in the 2D case the particles are free to move from one stripe to another one but such transitions happened to be rare due to repulsion between charges.

We note that the friction force for electrons on a surface of liquid helium can have a more complicated form due to various low energy excitations in this system (see, e.g., [2]). However, the Langevin approach reproduces well the thermal distribution in the system and we consider that this approach is reasonably justified as the first step to the investigation of this rather complex and nontrivial system. However, we suppose that future studies will allow us to test other forms of the friction force in the Langevin equation that will capture the specific features of electron friction on the surface of liquid helium due to rich properties of low energy excitations in this system.

Indeed, the results presented in Fig. 17 show that the temperature dependence of Wigner crystal velocity v_W is well described by the Arrhenius thermal activation equation that confirms that the Langevin approach provides us a reasonable description of the thermal environment.

The obtained results for v_W are not sensitive to the interaction radius between charges R_C as it is illustrated in Fig. 18

where it is changed by a factor 50 with practically the same profile of time dependence $v_W(t)$, up to statistical fluctuations. This is in agreement with the results of Fig. 2 which shows that the chain of charges, where all interactions are taken into account, is rather well described by the symplectic map with only nearby interactions between charges. We also note that the comparison between 1D chain dynamics with only nearest neighbors interactions and the chain with interactions of all charges had been performed in [13,23] showing that the short range approximation for interactions provides rather good approximation. In addition, we also show in Fig. 19 that the dependencies $v_W(E_{dc})$ for the 1D case (with only nearby interactions) and the 2D case (with 1 stripe/line) remain very close to each other. Thus the 1D case captures the main physical features of the system being very useful for the description of the 2D system.

Thus, we consider that the results discussed above justify the approximations used in our numerical simulations.

VIII. DISCUSSION

In this work we demonstrated that the Wigner crystal diode transport appears naturally for charge motion in asymmetric 1D and 2D potential. In the presence of charge interactions a dc field moves crystal easily in one direction while no current appears in the opposite direction. Our results show close similarities of diode transport in 1D and 2D. The diode transport appears in the Aubry pinned phase.

We think that the asymmetry is rather natural for various materials since already three different atoms in a periodic cell create generally an asymmetric potential. An incommensurate charge density in such materials can be induced by effective charge doping from other planes (e.g., like in high-temperature cuprates superconductors) or impurities.

With recent progress in experimental studies of Aubry transition with cold ions [27,28] and colloidal monolayers [33] we hope to obtain a deeper understanding of mechanisms of nanofriction on an atomic scale [31]. These experiments can be also performed with asymmetric potentials providing first experimental realizations of Wigner crystal diode. Indeed, two-harmonic optical lattices had been already realized experimentally (see, e.g., [34,35]) which opens possibilities to study the diode regime with cold ions. The dependence of the Aubry transition on density, obtained in [13] (see (5) and [44]), shows that the Aubry phase can be reached with a moderate amplitude of lattice potential created by laser fields. Indeed, for $\nu \approx 0.38$ we obtain from (5) $K_{cv} \approx 0.00044$ with the required potential amplitude of Aubry transition being $V_A = K_{cv}e^2/(\ell/2\pi) \approx 0.04$ K for the lattice period $\ell \sim 1 \mu\text{m}$ ($V_A \approx 3$ K for $\nu = 1.618$).

In addition to cold ion experiments we think that there are promising possibilities to study the Wigner crystal diode with electrons on liquid helium moving in a quasi-1D channel [7]. The first experiments in this direction have been reported recently in [53]. According to the above estimate, for electron density $\nu \approx 1.618$ and $\ell \approx 1 \mu\text{m}$ the Aubry transition takes place at the potential amplitude $V_A \approx 3$ K that is well below the electron temperature of about 0.1 K well available for such experiments (see, e.g., [7,53]).

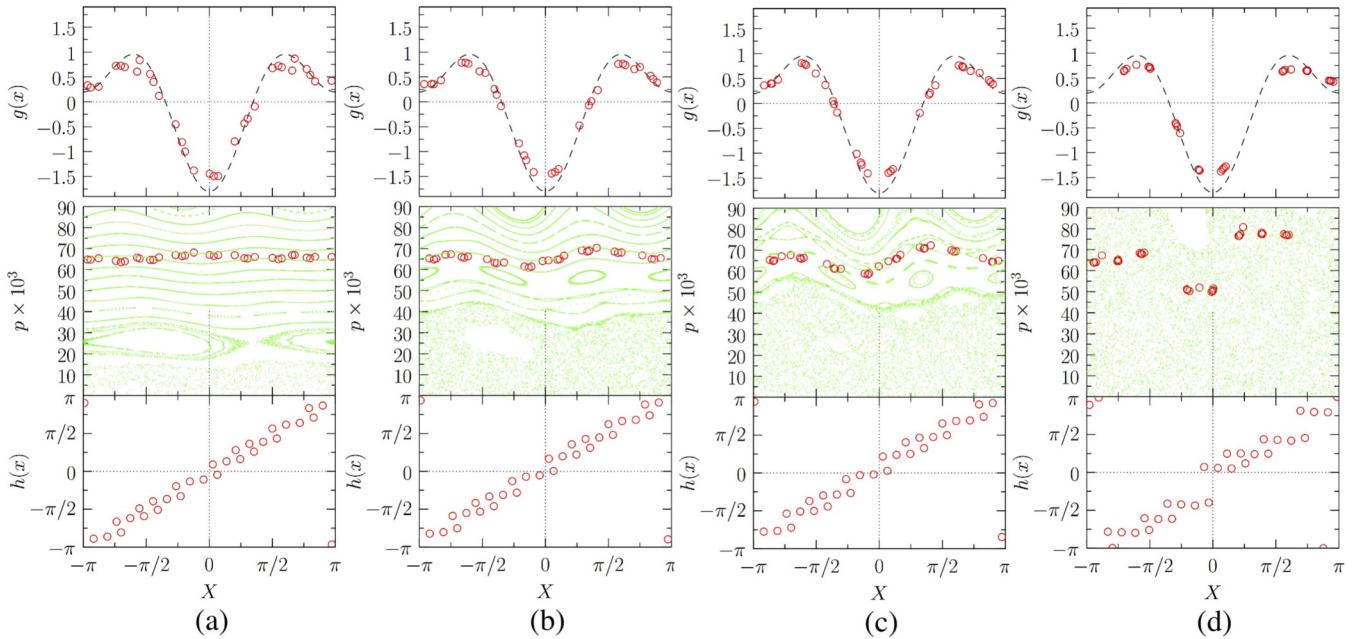


FIG. 13. Same as in Fig. 2 but for $\nu \approx 1.618$ with $N = 89$ charges for $L = 51$ potential periods and $K = 0.002$ (a), $K = 0.005$ (b), $K = 0.008$ (c), and $K = 0.02$ (d).

There are also possibilities of experimental realization of a Wigner crystal diode with colloidal monolayers extending the experiments [33] to asymmetric potentials.

We expect that the experimental investigations of electron and ion transport in a periodic potential at low temperatures will allow us to understand the nontrivial mechanisms of friction and thermoelectricity at nanoscale and then on atomic scale with new applications for material science.

ACKNOWLEDGMENTS

We thank N. Beysengulov, A. D. Chepelienskii, J. Lages, D. A. Tayurskii, and O. V. Zhirov for useful remarks and discussions. This work was supported in part by the Programme Investissements d'Avenir ANR-11-IDEX-0002-02, Reference ANR-10-LABX-0037-NEXT France (Project

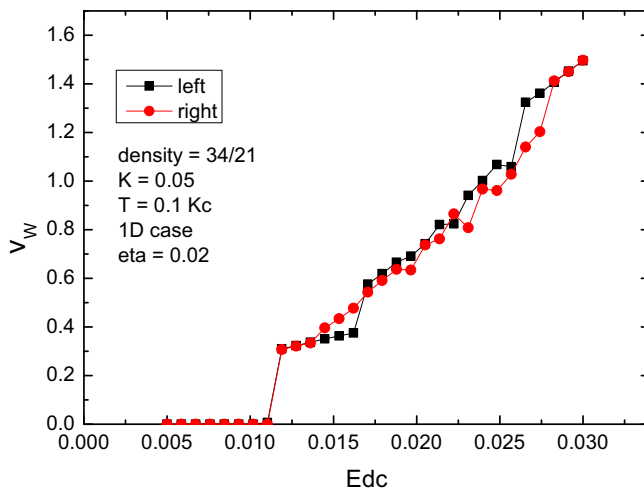


FIG. 14. Same as in Fig. 7(b) but at $\eta = 0.02$ (instead of $\eta = 0.1$).

THETRACOM). This work was granted access to the HPC GPU resources of CALMIP (Toulouse) under the allocation 2018-P0110. The development of the VexCL library was partially funded by the state assignment to the Joint supercomputer center of the Russian Academy of sciences for scientific research. The work of M. Y. Zakharov was partially funded by the subsidy allocated to Kazan Federal University for the state assignment in the sphere of scientific activities (Project No. 3.9779.2017/8.9).

APPENDIX

Here we present Figs. 13, 14, 15, 16, 17, 18, and 19 complementing the main text of the paper.

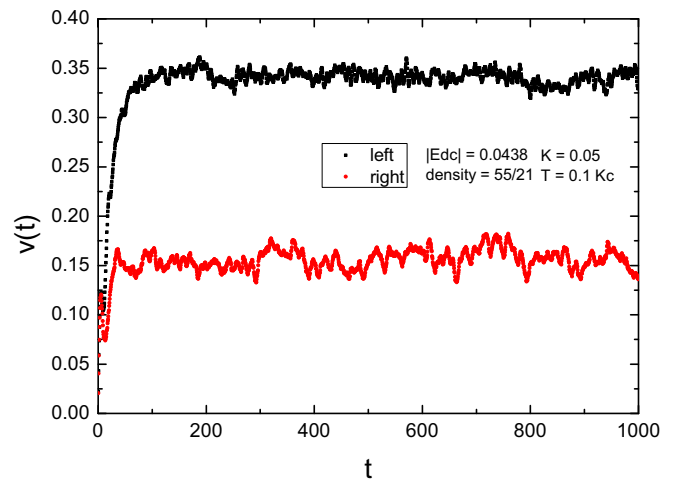


FIG. 15. Time dependence of velocity in x in 2D with $N_s = 5$ stripes; here $\nu = N/L = 55/21$, $K = 0.05$, $T = 0.1K_c = 0.00462$, $\eta = 0.1$, $|E_{dc}| = 0.0438$. The time averaged Wigner crystal velocities are $v_W = v_{\text{left}} = -0.34$ and $v_W = v_{\text{right}} = 0.16$.

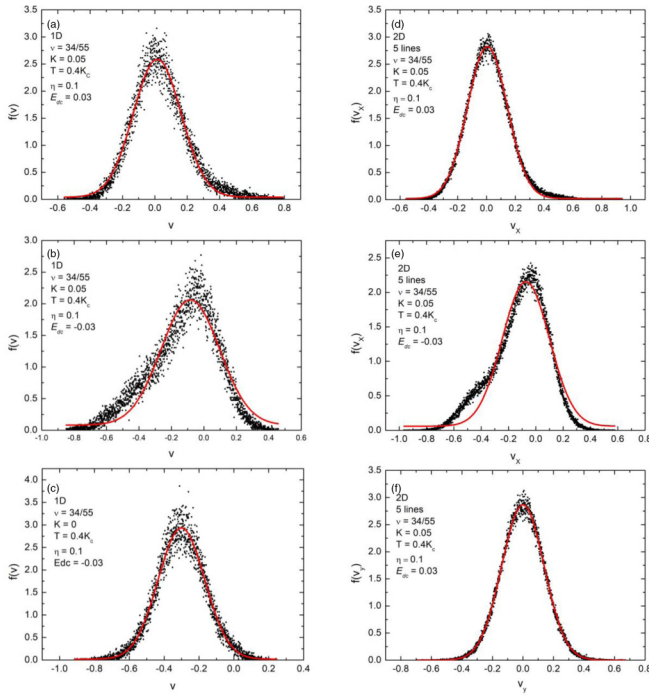


FIG. 16. Verification of the thermalization of charges in 1D and 2D (5 stripes/lines), black points show particle velocities in the time range $200 \leq t \leq 300$, the red curve shows the theoretical thermal Maxwell distribution centered at the average velocity of particles v_W in x direction. System parameters are given in the figure panels.

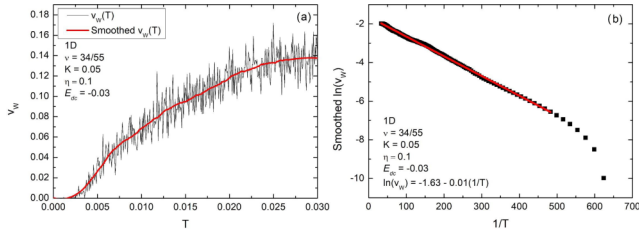


FIG. 17. Dependence of the Wigner crystal velocity v_W on temperature T in the 1D case. (a) Numerical results for v_W are shown by small points connected by the black curve, and the red curve shows the smoothed dependence obtained by the Savitzky-Golay filter with polynomial order 2 (points of window 50 in ORIGIN package). (b) Black squares show data for the smoothed red curve of (a), the red line shows the Arrhenius thermal activation dependence with the fit parameters $\ln v_W = -0.163 - A_r/T$ at the activation energy $A_r = 0.01$. The system parameters are given in the panels.

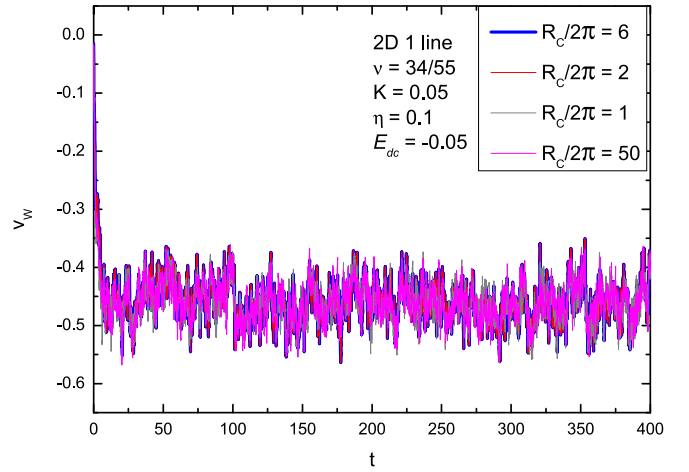


FIG. 18. Dependence of v_W on time t in the 2D case (1 stripe/line, velocity is in x direction) for different values of interaction radius $R_C/2\pi = 1, 2, 6$ (our main case), 50; system parameters are given in the panel.

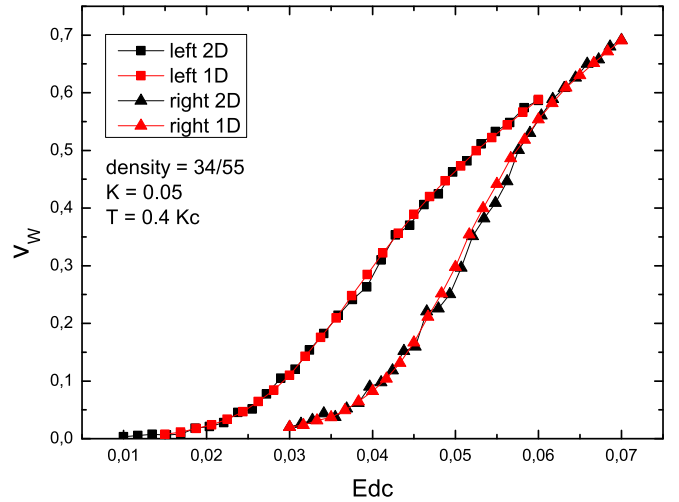


FIG. 19. Dependence of v_W on E_{dc} for the 1D case and 2D case (1 stripe/line; $R_C/2\pi = 6$, velocity is in x direction); system parameters are given in the figure panel.

[1] E. Wigner, On the interaction of electrons in metals, *Phys. Rev.* **46**, 1002 (1934).
 [2] Y. Monarkha and K. Kono, *Two-Dimensional Coulomb Liquids and Solids* (Springer, Berlin, 2004).
 [3] J. S. Meyer and K. A. Matveev, Wigner crystal physics in quantum wires, *J. Phys.: Condens. Matter* **21**, 023203 (2009).
 [4] G. Birkl, S. Kassner, and H. Walther, Multiple-shell structures of laser-cooled $^{24}\text{Mg}^+$ ions in a quadrupole storage ring, *Nature (London)* **357**, 310 (1992).

[5] D. H. E. Dubin and T. M. O'Neil, Trapped nonneutral plasmas, liquids, and crystals (the thermal equilibrium states), *Rev. Mod. Phys.* **71**, 87 (1999).
 [6] V. E. Fortov, A. V. Ivlev, S. A. Khrapak, A. G. Khrapak, and G. E. Morfill, Complex (dusty) plasmas: Current status, open issues, perspectives, *Phys. Rep.* **421**, 1 (2005).
 [7] D. G. Rees, S.-S. Yeh, B.-C. Lee, K. Kono, and J.-J. Lin, Bistable transport properties of a quasi-one-dimensional Wigner solid on liquid helium under continuous driving, *Phys. Rev. B* **96**, 205438 (2017).

- [8] W. A. Little, Possibility of synthesizing an organic superconductor, *Phys. Rev.* **134**, A1416 (1964).
- [9] W. A. Little, Superconductivity at room temperature, *Sci. Am.* **212**, 21 (1965).
- [10] R. E. Thorne, Change-density-wave conductors, *Phys. Today* **5**, 42 (1996).
- [11] D. Jérôme, Historical approach to organic superconductivity, in *The Physics of Organic Superconductors and Conductors*, edited by A. Lebed (Springer, Berlin, 2008), p. 3.
- [12] S. A. Brazovskii, Ferroelectricity and charge ordering in quasi-1D organic conductors, in Ref. [11], p. 313.
- [13] I. Garcia-Mata, O. V. Zhirov, and D. L. Shepelyansky, Frenkel-Kontorova model with cold trapped ions, *Eur. Phys. J. D* **41**, 325 (2007).
- [14] O. M. Braun and Yu. S. Kivshar, *The Frenkel-Kontorova Model: Concepts, Methods, Applications* (Springer, Berlin, 2004).
- [15] B. V. Chirikov, A universal instability of many-dimensional oscillator systems, *Phys. Rep.* **52**, 263 (1979).
- [16] A. J. Lichtenberg and M. A. Lieberman, *Regular and Chaotic Dynamics* (Springer, Berlin, 1992).
- [17] J. D. Meiss, Symplectic maps, variational principles, and transport, *Rev. Mod. Phys.* **64**, 795 (1992).
- [18] B. Chirikov and D. Shepelyansky, Chirikov standard map, *Scholarpedia* **3**, 3550 (2008).
- [19] V. L. Pokrovsky and A. L. Talapov, *Theory of Incommensurate Crystals* (Harwood Academic, New York, 1984).
- [20] S. Aubry, The twist map, the extended Frenkel-Kontorova model, and the devil's staircase, *Physica D* **7**, 240 (1983).
- [21] O. V. Zhirov and D. L. Shepelyansky, Wigner crystal in snaked nanochannels, *Eur. Phys. J. B* **82**, 63 (2011).
- [22] O. V. Zhirov and D. L. Shepelyansky, Wigner crystal in snaked nanochannels: Outlook, *Physica B* **407**, 1909 (2012).
- [23] O. V. Zhirov and D. L. Shepelyansky, Thermoelectricity of Wigner crystal in a periodic potential, *Europhys. Lett.* **103**, 68008 (2013).
- [24] J. He and T. M. Tritt, Advances in thermoelectric materials research: Looking back and moving forward, *Science* **357**, eaak9997 (2017).
- [25] T. Pruttivarasin, M. Ramm, I. Talukdar, A. Kreuter, and H. Haffner, Trapped ions in optical lattices for probing oscillator chain models, *New J. Phys.* **13**, 075012 (2011).
- [26] A. Bylinskii, D. Gangloff, and V. Vuletic, Tuning friction atom-by-atom in an ion-crystal simulator, *Science* **348**, 1115 (2015).
- [27] A. Bylinskii, D. Gangloff, I. Countis, and V. Vuletic, Observation of Aubry-type transition in finite atom chains via friction, *Nat. Mater.* **11**, 717 (2016).
- [28] J. Kiethe, R. Nigmatullin, D. Kalincev, T. Schmirander, and T. E. Mehlstaubler, Probing nanofriction and Aubry-type signatures in a finite self-organized system, *Nat. Commun.* **8**, 15364 (2017).
- [29] E. Shimshoni, G. Morigi, and S. Fishman, Quantum Zigzag Transition in Ion Chains, *Phys. Rev. Lett.* **106**, 010401 (2011).
- [30] A. Benassi, A. Vanossi, and E. Tosatti, Nanofriction in cold ion traps, *Nat. Commun.* **2**, 236 (2011).
- [31] D. Mandelli and E. Tosatti, Microscopic friction emulators, *Nature (London)* **526**, 332 (2015).
- [32] N. Manini, G. Mistura, G. Paolicelli, E. Tosatti, and A. Vanossi, Current trends in the physics of nanoscale friction, *Adv. Phys.* **X 2**, 569 (2017).
- [33] T. Brazda, A. Silva, N. Manini, A. Vanossi, R. Guerra, E. Tosatti, and C. Bechinger, Experimental Observation of the Aubry Transition in Two-Dimensional Colloidal Monolayers, *Phys. Rev. X* **8**, 011050 (2018).
- [34] G. Roati, C. D'Errico, L. Fallani, M. Fattori, C. Fort, M. Zaccanti, G. Modugno, M. Modugno, and M. Inguscio, Anderson localization of a non-interacting Bose-Einstein condensate, *Nature (London)* **453**, 895 (2008).
- [35] M. Schreiber, S. S. Hodgman, P. Bordia, H. P. Luschen, M. H. Fischer, R. Vosk, E. Altman, U. Schneider, and I. Bloch, Observation of many-body localization of interacting fermions in a quasirandom optical lattice, *Science* **349**, 842 (2015).
- [36] F. Braun, Ueber die stromleitung durch schwefelmetalle, *Ann. Phys. Chem.* **229**, 556 (1875).
- [37] P. Horowitz and W. Hill, *The Art of Electronics* (Cambridge University Press, Cambridge, UK, 1989).
- [38] S. Lepri, R. Livi, and A. Politi, Thermal conduction in classical low-dimensional lattices, *Phys. Rep.* **377**, 1 (2003).
- [39] K. Ahnert and M. Mulansky, Odeint—solving ordinary differential equations in C++, *AIP Conf. Proc.* **1389**, 1586 (2011).
- [40] D. Demidov, K. Ahnert, K. Rupp, and P. Gottschling, Programming CUDA and OpenCL: A case study using modern C++ Libraries, *SIAM J. Sci. Comput.* **35**, C453 (2013).
- [41] D. Demidov, VEXCL, <https://github.com/ddemidov/vexcl>. Accessed Dec. 2018.
- [42] K. Ahnert, D. Demidov, and M. Mulansky, Solving ordinary differential equations on GPUs, in *Numerical Computations with GPUs*, edited by V. Kindratenko (Springer, Berlin, 2014), pp. 125–157.
- [43] Olympe, CALMIP <https://www.calmip.univ-toulouse.fr/spip.php?article582>. Accessed Dec. 2018.
- [44] O. V. Zhirov, J. Lages, and D. L. Shepelyansky, Thermoelectricity of cold ions in optical lattices, [arXiv:1901.09588](https://arxiv.org/abs/1901.09588).
- [45] E. M. Lifshits and L. P. Pitaevskii, *Physical Kinetics* (Pergamon Press, Oxford, UK, 1981).
- [46] R. P. Feynman, R. B. Leighton, and M. Sands, *The Feynman Lectures on Physics* (Addison Wesley, Reading, MA, 1963), Vol. 1, Chap. 46.
- [47] F. Julicher, A. Ajdari, and J. Prost, Modeling molecular motors, *Rev. Mod. Phys.* **69**, 1269 (1997).
- [48] R. D. Astumian and P. Hanggi, Brownian motors, *Phys. Today* **55**, 33 (2002).
- [49] A. D. Chepelianskii, M. V. Entin, L. I. Magarill, and D. L. Shepelyansky, Photogalvanic current in artificial asymmetric nanostructures, *Eur. Phys. J. B* **56**, 323 (2007).
- [50] K. Moskvovtsev and M. I. Dykman, Self-diffusion in a spatially modulated system of electrons on helium, [arXiv:1808.10779](https://arxiv.org/abs/1808.10779).
- [51] N. Li, J. Ren, L. Wang, G. Zhang, P. Hanggi, and B. Li, Phononics: Manipulating heat flow with electronic analogs and beyond, *Rev. Mod. Phys.* **84**, 1045 (2012).
- [52] See Supplemental Material at <http://link.aps.org/supplemental/10.1103/PhysRevB.99.155416> for a video of Wigner crystal motion. (See also <http://www.quantware.ups-tlse.fr/QWLIB/wignerdiode/>.)
- [53] J.-Y. Lin, A. V. Smorodin, A. O. Badrutdinov, and D. Konstantinov, Transport properties of a quasi-1D Wigner solid on liquid helium confined in a microchannel with periodic potential, *J. Low Temp. Phys.* (2018), doi:[10.1007/s10909-018-2089-7](https://doi.org/10.1007/s10909-018-2089-7)